Electronic Supplementary Material (ESI) for Physical Chemistry Chemical Physics.

Supplementary Information

Theoretical scheme of the nonvolatile strain switchable high/low resistance based on the novel strain-tunable magnetic anisotropy in $Mn_{2.25}Co_{0.75}Ga_{0.5}Sn_{0.5}$/MgO superlattice

Yuan Liu[a], Li Huang[a], Hongshuang Liu[a], Liying Wang[a,b*]

[a]*Tianjin Key Laboratory of Low Dimensional Materials Physics and Preparation Technology, School of Science, Tianjin University, Tianjin 300354, China*

[b]*Tianjin Demonstration Center for Experimental Physics Education, School of Science, Tianjin University, Tianjin 300354, China*

*Author to whom all correspondence should be addressed.

E-mail address: liying.wang@tju.edu.cn (Liying Wang)

Table S1. The calculated total magnetic moment M_{tot} (μ_B per cell), site-resolved magnetic moments M_z (μ_B per atom), formation energy ΔH_f (eV) and cohesive energy E_{coh} (eV) of MCGS alloy.

Alloy	M_{tot}	$M_{Mn(A)}$	$M_{Mn(B)}$	$M_{Mn(C)}$	M_{Co}	ΔH_f	E_{coh}
$Mn_{2.25}Co_{0.75}Ga_{0.5}Sn_{0.5}$	2.00	-1.74	3.04	-0.56	1.04	-0.59	-8.32

Table S1 shows the calculated total and atomic magnetic moments of MCGS alloy. The calculated total magnetic moment of MCGS is 2.00 μ_B. The site-resolved magnetic moments are $M_{Mn(A)}$=-1.74 μ_B, $M_{Mn(B)}$=3.04 μ_B, $M_{Mn(C)}$=-0.56 μ_B and M_{Co}=1.04 μ_B, resulting in a ferrimagnetic state with antiparallel coupling of the moments at the nearest neighboring Mn atoms, which is similar with the magnetic configuration of the reported Mn_2CoAl alloy [*Phys. Rev. Lett*. 2013, **110**, 100401-100405].

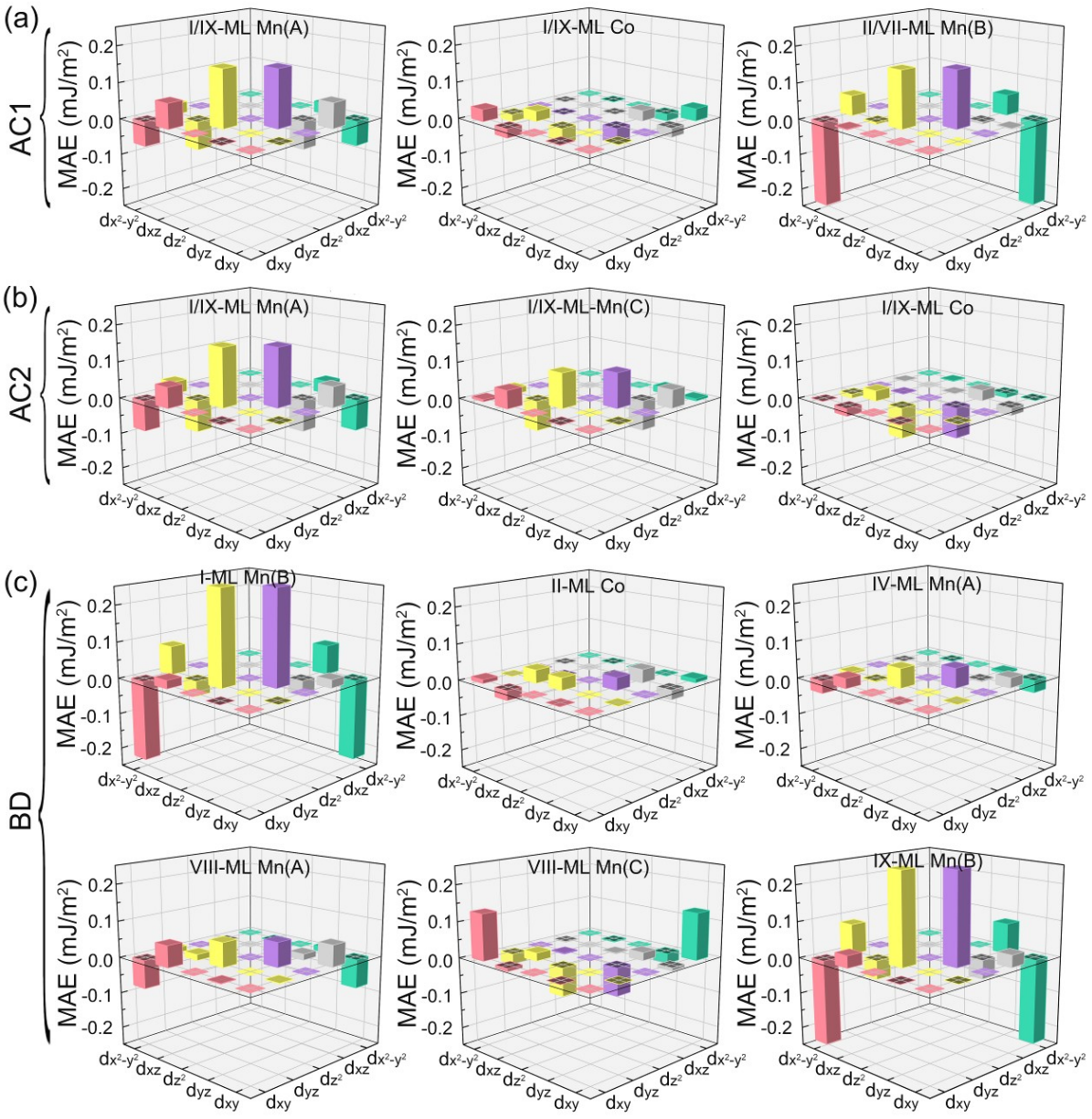

Fig. S1 Orbital-resolved MAE of Mn(A), Mn(B), Mn(C) and Co-*d* orbitals of $(MCGS)_2/(MgO)_1$ superlattices with (a) AC1, (b) AC2 and (c) BD terminations. I/IX, II/VII, IV and VIII refer to the layer numbers of MCGS.

Fig. S1 shows the calculated orbital-resolved MAE to further elucidate the physical mechanism of the interfacial PMA in AC1, AC2, and BD models. In AC1 model (Fig. S1a), we can find that the matrix element difference between d_{yz} and d_{z^2} orbitals of the interfacial I/IX-ML Mn(A) atoms contribute significant PMA to the system, while the rest of the Mn(A)-*d* orbitals

devotes small negative/positive MAE which almost cancels each other out. For II/VII-ML Mn(B) atoms, the d_{yz} and d_{z^2} orbitals also contribute obvious PMA, while the d_{xy} and $d_{x^2-y^2}$ orbitals contribute slightly larger negative IMA Therefore, II/VII-ML Mn(B) shows weak IMA. Thus, the positive PMA in AC1 model mainly derives from d_{yz} and d_{z^2} orbitals of the interfacial I/IX-ML Mn(A) atoms. In AC2 model, the MAE contribution of I/IX-MLs Mn(A) is similar to that in AC1 model. The decrease of the PMA in AC2 model can be attributed to the dominant contribution of d_{yz} and d_{z^2} orbitals of I/IX-MLs Co atoms which present obvious IMA, as shown in Fig. S1b. Compared with AC1 and AC2 models, the significant large PMA of I-ML Mn(B) atoms in BD model mainly arises from the increasing PMA contribution of d_{yz} and d_{z^2} orbitals. In addition, for BD model, the IMA from matrix element differences between d_{yz} and d_{xy} of II-ML Co atoms decreases to almost zero, while the d_{yz} and d_{z^2} orbitals turns to show PMA, as shown in Fig. S1c. Our results show that the interfacial Mn atoms prefer to contributing PMA, which also indicates that the termination of the interfaces is a critical factor to the MAE of $(MCGS)_2/(MgO)_1$ superlattices.

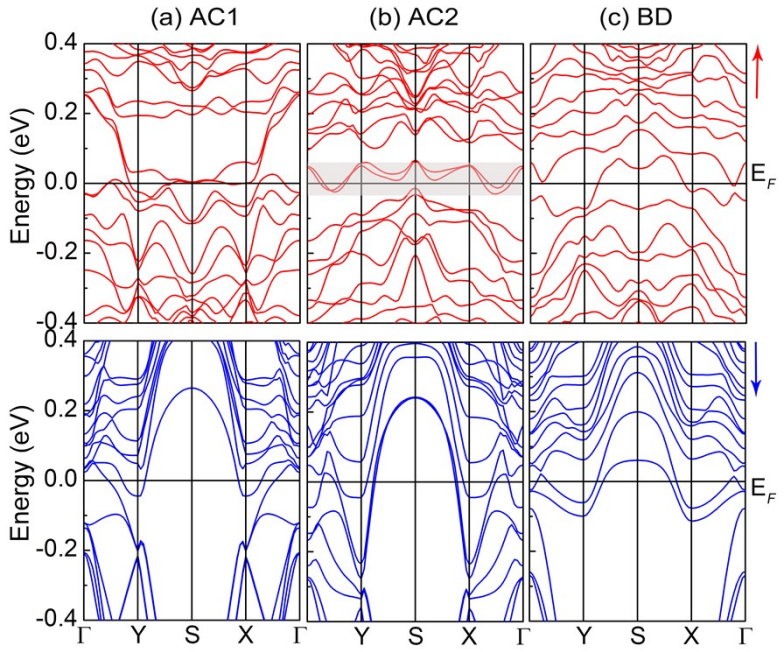

Fig. S2 Band structures of $(MCGS)_2(MgO)_1$ superlattices with (a) AC1-, (b) AC2-, and (c) BD-type terminations. The red and blue lines represent the majority- and minority-spin channels, respectively.

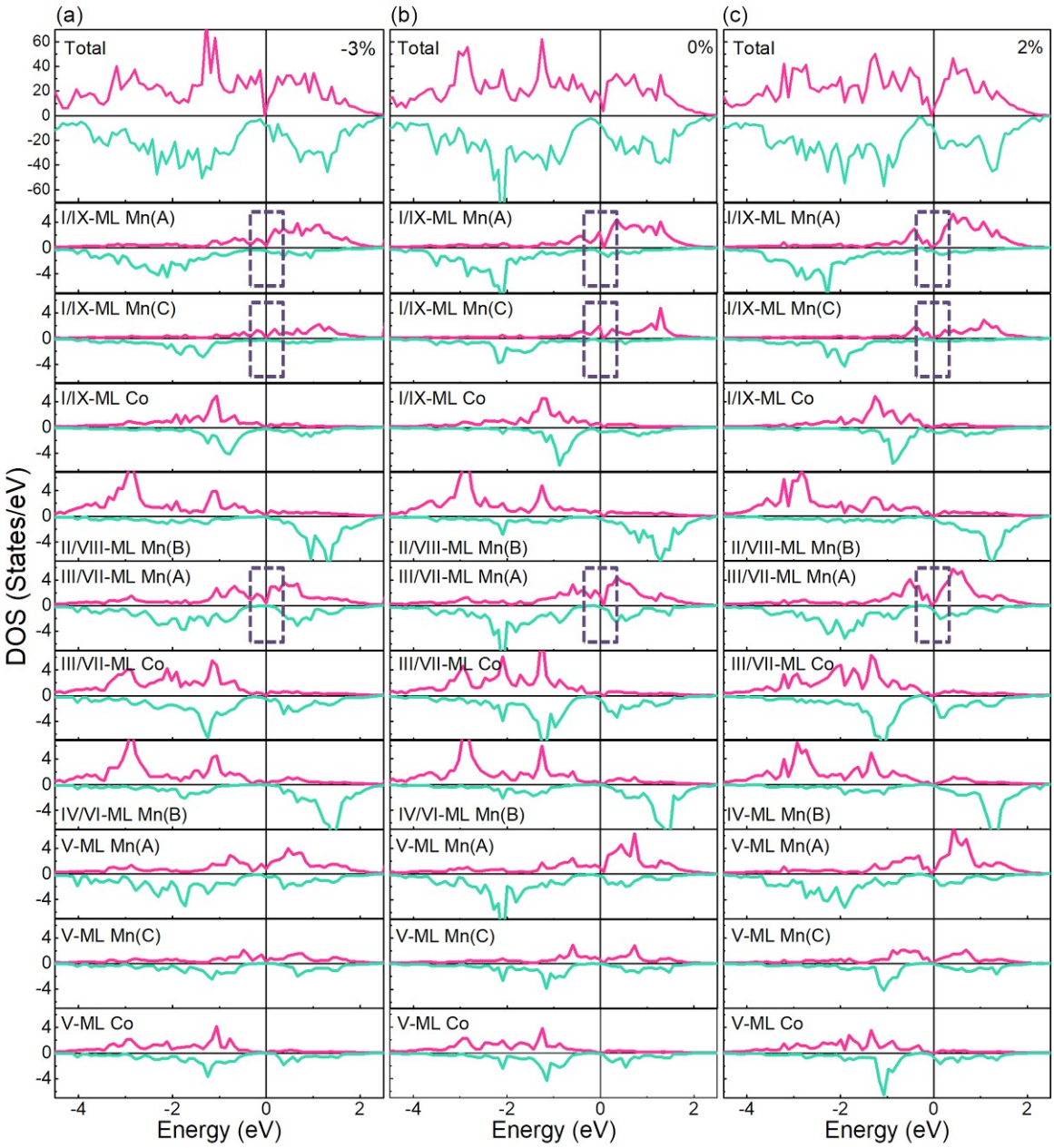

Fig. S3 Total and partial DOS of AC2-terminated $(MCGS)_2/(MgO)_1$ superlattice under -3%, 0% and 2% strains.

The interfacial lattice deformation occurs during applying tensile/compressive strain. Owing to the interfacial lattice deformation, the inter-atomic hybridization interaction and intra-atomic exchange interaction in the lattice will be affected, which will influence the energy dispersion of the electronic structures in the two spin directions.

To further understand the changes of the electronic structures around Fermi level, we calculate

the total and partial density of states (DOS) of AC2-terminated $(MCGS)_2/(MgO)_1$ superlattice under different strains. Figs. S3a-c show the total and partial DOS of AC2 model under -3%, 0% and 2% strains. From the total DOS of unstrained AC2 model (0% strain), we can clearly observe that the Fermi level locates at the shoulder of a peak around Fermi level in the majority-spin channel. There is an obvious narrow energy gap at about 0.06 eV above Fermi level, which is consistent with the discussions on the band structures shown in Fig. S2. Here, we should note that the another energy gap below the Fermi level as described in Fig. S3 can not be seen in the total DOS because the gap is almost a zero gap. From the partial DOS of I~IX-ML Mn and Co atoms, as shown in Fig. S3b, one can see that the peak around Fermi level arises primarily from the interfacial I/IX-ML, III/VII-ML Mn(A) and Mn(C) [see the dash boxes shown in Fig. S3b]. In Fig. S3c, when the tensile strain is applied, the majority-spin states of I/IX-ML, III/VII-ML Mn(A) and Mn(C) atoms tend to move towards higher energy region, and the Fermi level just falls into the energy gap under 1%~2% tensile strains, while the minority-spin states move to the opposite lower energy direction. Then, the larger spin splitting in DOS between majority- and minority-spin states of I/IX-ML, III/VII-ML Mn(A) and Mn(C) atoms occurs which derives from the enhanced intra-atomic exchange interaction under the tensile strains. In contrast, for the compressive strained case (see Fig. S3a), the spin splitting of I/IX-ML, III/VII-ML Mn(A) and Mn(C) atoms is weakened. We can find that the majority-spin states of I/IX-ML, III/VII-ML Mn(A) and Mn(C) atoms move towards lower energy region, while the minority-spin states move towards higher energy direction. For the cases of AC2 models under -3%~-5% compressive strains, Fermi level exactly falls into the energy gap in the majority-spin channel. The change of the spin splitting of I/IX-ML, III/VII-ML Mn(A) and Mn(C) atoms is also consistent to the change of the site-resolved magnetic moments shown in Table S2.

Table S2. The calculated site-resolved magnetic moments M (μ_B per atom) of AC2-terminated $(MCGS)_2/(MgO)_1$ superlattice under -3%, 0%, and 2% strains.

Atom	Layer	M (-3% compressive strain)	M (0%)	M (2% tensile strain)
Mn(A)	I/IX	-2.71	-2.95	-3.10
Mn(C)		-2.21	-2.60	-2.82
Co		0.68	0.81	0.85
Mn(B)	II/VIII	2.99	3.19	3.30
Mn(A)	III/VII	-1.21	-1.57	-2.02
Co		0.95	1.09	1.16
Mn(B)	IV/VI	2.86	3.08	3.22
Mn(A)	V	-1.51	-1.88	-2.16
Mn(C)		-0.68	-0.60	-0.42
Co		0.89	1.03	1.11

As shown in Table S2, for AC2-terminated $(MCGS)_2/(MgO)_1$ superlattice, it can be clearly seen that the negative magnetic moments of the interfacial Mn and Co (I-III and VII-IX layers) exhibits an obvious change compared with the MCGS bulk, which can be attributed to the strong exchange interactions between the interfacial atoms. However, for the inner MCGS layers (IV-VI layers), the magnetic moments of Mn and Co atoms are almost the same as that in MCGS bulk. The strong interfacial interaction is the key factor for the decrease of the spin polarization in MCGS/MgO superlattice. In detail, when the tensile strain is applied, the negative and positive magnetic moments of Mn and Co atoms on the interfacial I-III layer tend to increase further compared with the unstrained MCGS/MgO superlattice (see Table S2). Conversely, the magnetic moments of the interfacial Mn and Co atoms tend to decrease under compressive strain. As discussed in Fig. 5, for AC2 model, the Fermi level tend to move towards the opposite energy

directions in majority spin under tensile and compressive strains, and finally locates in the upper or lower energy gap. The changes of the electronic structure under strains are consistent with the mangentic moments change trend of the interficial Mn and Co atoms.